

Universal molecular-confined synthesis of interconnected porous metal oxides-N-C frameworks for electrocatalytic water splitting

Bo You^{a,*}, Yadong Zhang^b, Peiqun Yin^a, De-en Jiang^{b,*}, and Yujie Sun^{c,*}

^aDepartment of Chemistry, University of Science and Technology of China, Hefei, Anhui 230026, China.

E-mail: youbo@mail.ustc.edu.cn

^bDepartment of Chemistry, University of California, Riverside, California 92521, United States.

E-mail: djiang@ucr.edu

^cDepartment of Chemistry and Biochemistry, Utah State University, Logan, Utah 84322, United States.

E-mail: yujie.sun@usu.edu

Keywords: (water splitting; porous frameworks; electrocatalysis; nonprecious; theory modeling)

Abstract

The rational synthesis of high performance electrocatalysts at low cost for water splitting (hydrogen and oxygen evolution reaction, HER and OER) is highly desirable but remains a key challenge. Herein, we report a versatile molecular-confining route to construct strongly coupled metal oxides-N-C frameworks with interconnected configuration. By simply chelating various transition metal ions with ethylenediaminetetraacetic acid disodium salt (EDTA) in agarose hydrogel and subsequently carbonization, the high specific surface area porous N-C frameworks with strongly coupled metal oxides (e.g., manganese, iron, cobalt, nickel and their mixed oxides) can be prepared as advanced nonprecious water splitting electrocatalysts. For instance, the resulting Co_3O_4 -N-C frameworks with the high surface area of $153 \text{ m}^2 \text{ g}^{-1}$, and the moderate nitrogen content of 1.23%, require an overpotential of 324 mV to afford a current density of 10 mA cm^{-2} in 0.1 M KOH for OER, superior to commercial RuO_2 catalysts. Density functional theory (DFT) calculations reveal that the strong coupling between N-C and Co_3O_4 tunes the local electronic structure of Co for high-valence active sites and assures optimal adsorption energies of OER intermediates. Moreover, Co_2P -N-C electrocatalysts derived from Co_3O_4 -N-C also exhibit excellent HER performance under 1.0 M KOH with a low overpotential of 139 mV to reach 10 mA cm^{-2} , a small Tafel slope of $45 \text{ mV decade}^{-1}$ and impressive stability, underscoring the versatility of our synthetic strategy.

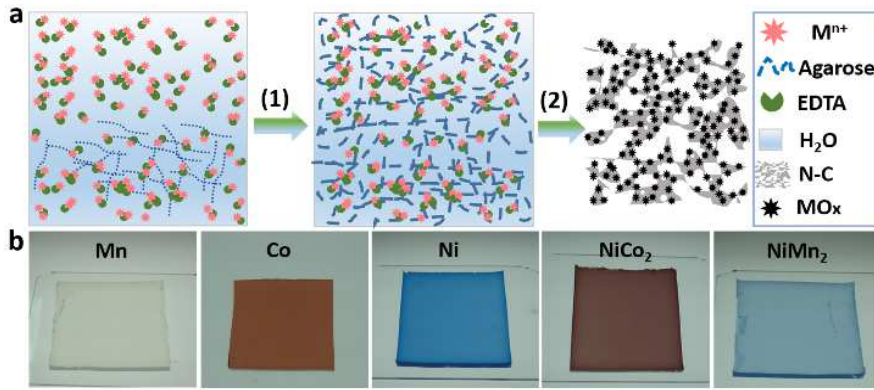
1. Introduction

Depletion of fossil fuels and potential climate change resulting from fossil fuel consumption have triggered a considerable interest in exploring sustainable energy resources and various energy storage/utilization techniques including metal-air batteries, water splitting devices, and fuel cells [1-4]. In particular, electrochemical water splitting is a practical and environmentally friendly approach to generate clean H_2 fuel, wherein, electrocatalysts play key roles in both H_2 and O_2 evolution reactions (HER and OER) during the overall water splitting [5-13]. It has been a long-standing challenge to

develop low-cost, efficient and durable electrocatalysts for water electrolysis under ambient conditions [14-19].

Most recent efforts have mainly focused on transition metal-based compounds owing to their low-cost, diversity, potential stability and theoretically high catalytic activity [14-19]. To accelerate the catalytic reaction kinetics and improve the efficiency, an optimal and rationally designed reaction interface is essential for the intrinsically triphase reactions of water electrolysis (solid, liquid and gas) [17]. For example, Shao-Horn et al. suggested that integrating rare earth or alkaline earth metals with transition metal oxides would optimize the occupancy of 3d electron with an e_g symmetry of surface transition metal cations and enhance their intrinsic OER activity in alkaline solution (O_2 -saturated 0.1 M KOH) [20,21]. Sargent's group recently demonstrated that incorporating judicious combinations of Co, Fe and non-metal P can beneficially modulate the electronic structure of Ni sites for the formation of high valence active sites (Ni^{4+}) and thus significantly improve their OER activity under pH-neutral media (CO_2 -saturated 0.5 M $KHCO_3$ aqueous electrolyte) [4]. Moreover, our recent work showed that surface-modified N atoms are able to significantly improve the HER activity of metallic Ni under neutral condition (1 M pH=7 phosphate buffer) by simultaneously favoring the initial water adsorption and facilitating the following dissociation of water on Ni surface, which was also supported by density functional theory (DFT) calculations [10]. However, these aforementioned electrocatalysts usually suffer from electrode kinetic issues due to low specific surface area and/or poor conductivity of semiconducting metal oxides [17]. Consequently, in order to promote the accessibility of active sites, multiphase reactants/products transport, and electrons shuttle, great efforts have been directed towards synthesis of nanocarbon-based hybrids with high specific surface area, tailored pore configuration, and superior conductivity [7]. A few successful examples are Co_3O_4/N -rmGO [22], NiO/Ni -CNT [23], $Co_4N/CNW/CC$ [24], S,N-Fe/N/C-CNT [25] and $Co-C_3N_4$ [26]. Nevertheless, the practical application of these catalysts is still hindered by the costly and tedious multistep preparations and/or micro-structural non-homogeneity because of their heterogeneous synthetic routes [25,27,28]. For instance, Zhang and co-workers proposed a strategy for in-situ coupling of strung Co_4N and intertwined N-C fibers by electrodeposition of polypyrrole nanofibers on carbon cloths, growth of ZIF-67 wrapped on polypyrrole nanofibers, and final carbonization under N_2 atmosphere [24]. Wu's group reported the atomically dispersed $Fe-N_x$ species on N and S co-decorated hierarchically carbon layers (S,N-Fe/N/C-CNT) as efficient and durable bifunctional electrocatalysts for oxygen evolution and reduction reactions [25]. The S,N-Fe/N/C-CNT were prepared by coating CNTs with 2,2-bipyridine and Fe salt precursor, followed by pyrolysis at 900 °C under N_2 atmosphere and tedious acid leaching. During these synthetic processes, the insoluble carbon substrates such as carbon nanotube (CNT), and carbon cloth are usually employed for heterogeneously anchoring active components and repetitive rinsing steps are necessary to remove excess precursor solutions.

Herein, we demonstrate a universal, homogeneous and especially facile molecular-confining route to synthesize strongly coupled transition metal oxides and N-doped carbon frameworks with



Scheme 1. (a) Schematic illustration for the syntheses of metal oxides-nitrogen-carbon frameworks. Step (1) and (2) represent the gelation and carbonization, respectively. (b) Hydrogels with different transition metals.

interconnected configuration by simply chelating transition metal ions with ethylenediaminetetraacetic acid disodium salt (EDTA) in agarose hydrogel followed by carbonization (Scheme 1a, details available in Experimental section). Thanks to the coordination versatility of EDTA, this method is very general for fabricating multiple hydrogels (Scheme 1b) and thus the high specific surface area porous nitrogen-doped carbon frameworks with various strongly coupled metal oxides (e.g., Co₃O₄, NiO_x, MnO_x, NiCo_xO_y and NiMn_xO_y Fig. 1a-c and S1) can be readily obtained. Specifically, the coordination of EDTA with transition metal ions could not only suppress their hydrolysis, but also alleviate the agglomeration of metal oxide nanoparticles during carbonization due to the “molecular confinement effect” [29]. Meanwhile, EDTA can act as green N and C sources for in-situ incorporation with metal oxides. The agarose gel offers 3D hierarchically interconnected carbon frameworks to homogeneously anchor strongly coupled metal oxides in the final products, which promote the accessibility to metal oxide-N-C active sites. With these tailored nanoarchitecture, the resulting hybrids would exhibit excellent electrocatalytic performance. For example, the as-prepared Co₃O₄-N-C frameworks with a high surface area of 153 m² g⁻¹ and the moderate nitrogen content of 1.23% possess impressive electrocatalytic activity for OER in 0.1 M KOH, superior to commercial RuO₂ catalyst. Density functional theory (DFT) calculations suggest that the strong coupling between N-C and Co₃O₄ is able to provide suitable binding sites for OER intermediates, beneficial to the overall OER. Furthermore, the Co₂P-N-C electrocatalysts prepared by a low-temperature phosphidation of the Co₃O₄-N-C frameworks exhibit excellent electrocatalytic activity and impressive stability for HER in 1.0 M KOH.

2. Results and discussion

As a proof-of-concept, the Co₃O₄-N-C frameworks were firstly prepared. Scanning electron microscopy (SEM) reveals an interconnected, porous 3D carbon frameworks with continuous macropores in the micrometer size range (Fig. 1a). A closer inspection of the macropore walls in a high-magnification SEM image shows a mesoporous structure composed of stacked carbon nanoparticles (Fig. 1b). Transmission electron microscopy (TEM) characterization further validates

the hierarchical macropores (Fig. 1c, circle) interconnected with numerous mesopores (Fig. 1c, square). The absence of morphologically different particles indicates that all Co_3O_4 and N-C species are well integrated with each other, in sharp contrast to the EDTA-free counterpart which contains severely aggregated or very large Co-based nanoparticles (Fig. S2). Such a dramatic difference could be related to the molecular confinement effect of EDTA coordinating Co ions [29]. The high-resolution TEM (HR-TEM) image (Fig. 1d) presents apparently different domains of graphitic carbon and crystalline Co_3O_4 with clearly identified lattice fringe distance of 0.35 and 0.20 nm, corresponding to the (002) plane of graphite and the (400) plane of the cubic spinel Co_3O_4 , respectively. The high graphitization catalyzed by Co species is expected to provide excellent conductivity favorable for electrochemical applications [7]. To further investigate the well-integrated configuration of Co_3O_4 and N-C species, the Co_3O_4 -N-C were subjected to calcination in air to intentionally remove the N-C species, yielding pure Co_3O_4 . The morphology of the pure Co_3O_4 , as revealed by SEM (Fig. 1e) and TEM (Fig. 1f), is analogous to the mother Co_3O_4 -N-C (Fig. 1a-c), implying the homogeneous incorporation of Co_3O_4 in the N-C frameworks.

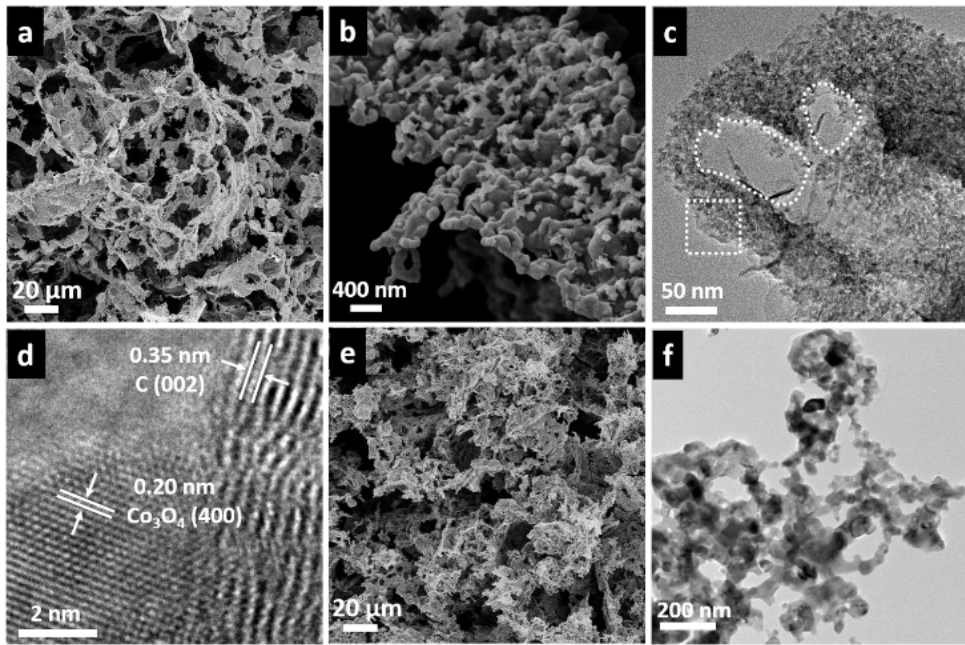


Fig. 1. (a, b) SEM, (c) TEM and (d) HR-TEM images of Co_3O_4 -N-C. (e) SEM and (f) TEM images of pure Co_3O_4 prepared by calcination of Co_3O_4 -N-C in air for removal of N-C species.

The XRD pattern of Co_3O_4 -N-C confirms the formation of cubic spinel Co_3O_4 and graphitic carbon (Fig. 2a), in consistent with the HR-TEM results (Fig. 1d). Inductively coupled plasma-atomic emission spectrometry reveals a Co content of 36.6 wt %. N_2 sorption isotherms (Fig. 2b) shows a typical type-IV curve with a distinct hysteresis loop close to H3 type [17,30-32]. The Brunauer-Emmett-Teller (BET) specific surface area and pore volume of Co_3O_4 -N-C were calculated to be 153 $\text{m}^2 \text{ g}^{-1}$ and 0.26 $\text{cm}^3 \text{ g}^{-1}$, respectively, further confirming the high porosity of Co_3O_4 -N-C. The corresponding pore size distribution curve derived from the adsorption branches of the isotherms by

using the Barrett-Joyner-Halenda (BJH) method clearly exhibits a large primary pore size of about 6.4 nm (Fig. 2b inset). X-ray photoelectron spectroscopy (XPS) analysis indicates that $\text{Co}_3\text{O}_4\text{-N-C}$ contains Co (12.41 at%), N (2.15 at%), C (56.84 at%), and O (28.6 at%) elements without other impurities (Fig. 2c). The high-resolution N 1s spectrum (Fig. 2c inset) could be fitted by three sub-peaks corresponding to pyridinic N (398.7 eV), pyrrolic N (400.0 eV), and graphitic (quaternary) N (401.1 eV) [15]. The content of N measured by element analysis is 1.23 wt%. Similarly, the high-resolution Co 2p spectrum (Fig. 2d) was deconvoluted into two peaks assignable to two pairs of spin-orbit doublets, indicating the coexistence of Co^{2+} and Co^{3+} and their four shakeup satellites (denoted as “sat” in Fig. 2d) [17]. In comparison to the XPS peak of Co 2p_{3/2} in pure Co_3O_4 , the positive shift of the corresponding peak of $\text{Co}_3\text{O}_4\text{-N-C}$ implies the close assembly and strong interaction between Co_3O_4 and N-C frameworks, resulting in the

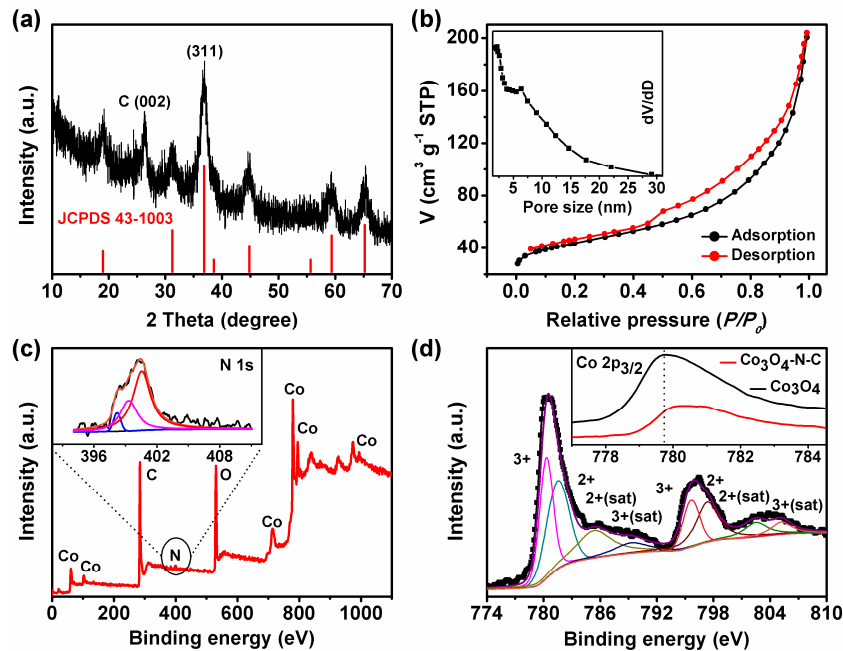


Fig. 2. (a) XRD pattern of $\text{Co}_3\text{O}_4\text{-N-C}$. (b) N_2 sorption isotherms and (inset) corresponding pore size distribution of $\text{Co}_3\text{O}_4\text{-N-C}$. (c) XPS survey spectrum and (inset) high resolution N 1s spectra of $\text{Co}_3\text{O}_4\text{-N-C}$. (d) High resolution Co 2p spectra and (inset) comparison of Co 2p_{3/2} spectra for $\text{Co}_3\text{O}_4\text{-N-C}$ and pure Co_3O_4 .

altered electron density of Co atoms with high valence due to the interface effect and then opening possibilities to tuning catalytic performance [4,33-36].

The electrocatalytic OER activity of $\text{Co}_3\text{O}_4\text{-N-C}$ was then investigated in alkaline solutions (0.1 M KOH) using a standard three-electrode system, in which a glassy carbon rotating disk electrode (RDE) loaded with different electrocatalysts was used as the working electrode (see details in the Experimental section). As shown in Fig. 3a, the polarization curve of $\text{Co}_3\text{O}_4\text{-N-C}$ shows a much earlier onset potential of ~ 1.47 V vs the reversible hydrogen electrode (RHE) and greater catalytic current than those of pure Co_3O_4 , N-C frameworks, and $\text{Co}_3\text{O}_4\text{+N-C}$ (prepared by post-impregnating a hydrogel-derived nanocarbon with the Co-EDTA complex followed by a similar carbonization process), highlighting the important role of the tailored nanostructure and the inherent coupling

between Co_3O_4 and the N-C frameworks in $\text{Co}_3\text{O}_4\text{-N-C}$. The best OER activity among the series of $\text{Co}_3\text{O}_4\text{-N-C}$ samples was achieved at pyrolysis temperature of 600 °C and the Co/agarose mass ratio of 1:1 (Fig. S3, $\text{Co}_3\text{O}_4\text{-N-C-600-1}$, denoted as $\text{Co}_3\text{O}_4\text{-N-C}$ for brevity). Noticeably, the OER current density of $\text{Co}_3\text{O}_4\text{-N-C}$ at the high potential also significantly exceeds those of commercial 20 wt% Pt/C and RuO_2 catalysts, despite its onset potential (~1.47 V) is slightly larger than that of RuO_2 (~1.46 vs RHE). More importantly, our $\text{Co}_3\text{O}_4\text{-N-C}$ affords a current density of 10 mA cm⁻² at a small

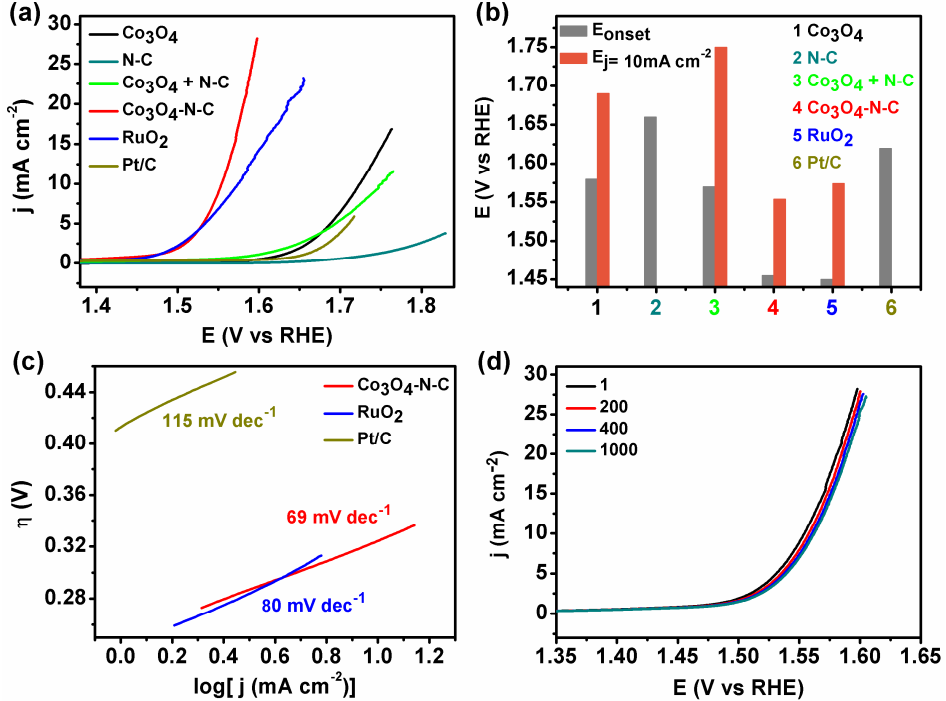


Fig. 3. (a) OER polarization curves in 0.1 M KOH at scan rate of 5 mV s⁻¹ and 1600 rpm. (b) Comparison of onset potentials and overpotentials at current density of 10 mA cm⁻². (c) Tafel plots and (d) Stability tests of $\text{Co}_3\text{O}_4\text{-N-C}$ electrocatalyst through potential cycling, in which the polarization curves before and after 1000 potential cycles are displayed. The loading of all the catalysts is 0.4 mg cm⁻².

overpotential (η) of 324 mV, even lower than that of RuO_2 (344 mV, Fig. 3b) and those of other reported nonprecious catalysts (Table S1) [19,37-42], such as $\text{CoS}_x\text{@PCN/rGO}$ (340 mV) [40], and NiN_4C_4 single atom catalysts even in 1.0 M KOH (331 mV) [43]. In addition, the smaller Tafel slope down to 69 mV dec⁻¹ compared to those of Pt/C (115 mV dec⁻¹) and RuO_2 (80 mV dec⁻¹) suggests its more favorable reaction kinetics (Fig. 3c).

Other than high activity, strong durability of an electrocatalyst is also of great significance for its practical application. Fig. 3d shows that, after 1000 potential cycles, the overpotential required to achieve the current density of 10 mA cm⁻² for $\text{Co}_3\text{O}_4\text{-N-C}$ only increases by less than 9 mV, indicating its superior stability. We believe that the unique properties of the proposed structural design endow $\text{Co}_3\text{O}_4\text{-N-C}$ with excellent electrocatalytic OER performance. Firstly, EDTA forms a stable coordination complex with Co^{2+} , responsible for a suppressed agglomeration of Co_3O_4 during high-temperature carbonization. Secondly, agarose gel offers 3D hierarchically interconnected carbon

frameworks with high surface area to homogeneously anchor the Co-EDTA complex, which promote the accessibility to metal oxide-nitrogen-carbon active sites and reduce ion transport resistance. Thirdly, the highly graphitic carbon frameworks formed by Co-catalyzed graphitization during

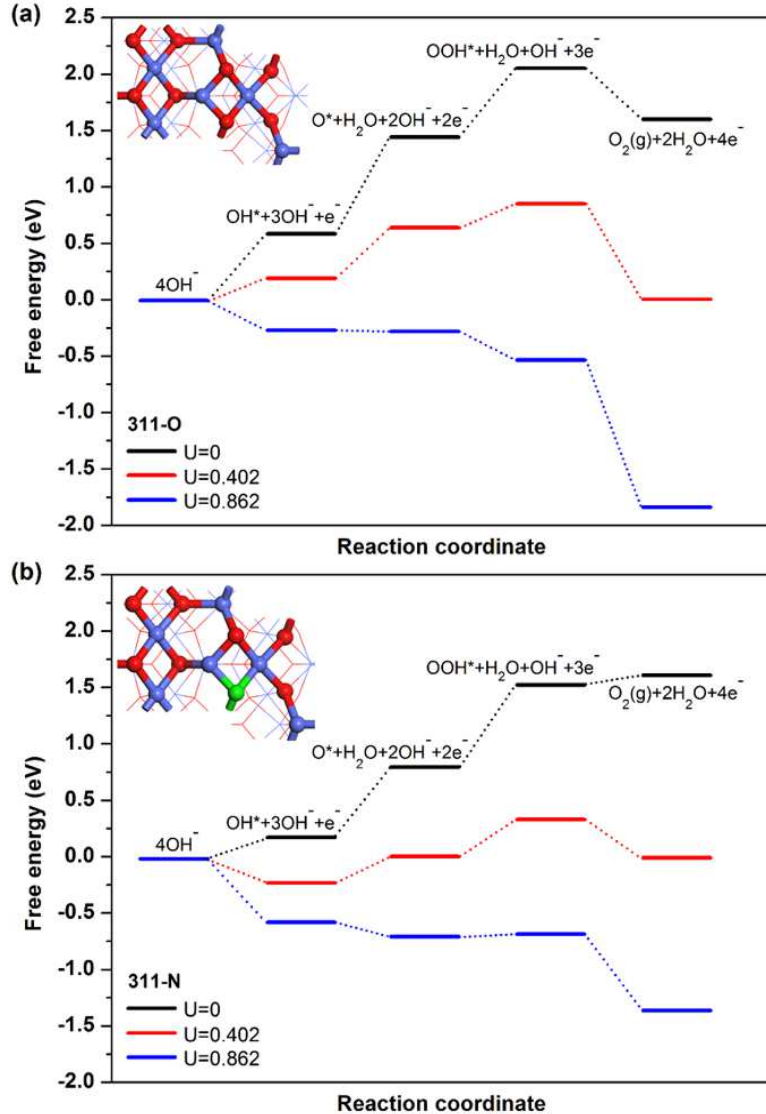


Fig. 4. Free energy diagrams of OER on facet 311 of (a) pure Co_3O_4 and (b) N-substituted Co_3O_4 for $\text{Co}_3\text{O}_4\text{-N-C}$ frameworks obtained at zero potential ($U=0$ V vs NHE), equilibrium potential ($U=0.402$ V vs NHE), and the potential ($U=0.862$ V vs NHE) for which all steps proceed downward at 0.1 M KOH and $T=298$ K. The insets show the models of the $\text{Co}_3\text{O}_4(311)$ and N-substituted $\text{Co}_3\text{O}_4(311)$. Colour code: blue, Co; Red, O; green, N.

carbonization facilitate electrons transport. Finally, the strongly coupling between the in-situ formed N-C frameworks and Co_3O_4 (as indicated by the positive shift of the $\text{Co} 2\text{p}_{3/2}$ XPS peak in $\text{Co}_3\text{O}_4\text{-N-C}$ compared to that of pure Co_3O_4 , Fig. 2d) may favorably affect the electronic structure of Co_3O_4 and thus assure optimal adsorption energies for OER intermediates.

In order to better understand this electronic effect on the OER activity of $\text{Co}_3\text{O}_4\text{-N-C}$, we calculated the energy profiles of several critical OER intermediates on $\text{Co}_3\text{O}_4\text{-N-C}$ via DFT. Pure Co_3O_4 was also included for comparison. The preferably exposed $\text{Co}_3\text{O}_4(311)$ and N-substituted $\text{Co}_3\text{O}_4(311)$ were

modeled for brevity (Fig. 4 inset). Under an equilibrium potential of 0.402 V vs NHE (normal hydrogen electrode), all reaction steps on $\text{Co}_3\text{O}_4(311)$ are thermodynamically uphill except for the last one (OOH^* desorption). The second step, which is 0.47 eV uphill, is considered to be the rate-determining-step (rds) of the overall OER (Fig. 4a). While for the N-substituted $\text{Co}_3\text{O}_4(311)$, the rds is the third step, which is 0.34 eV uphill, smaller than that on $\text{Co}_3\text{O}_4(311)$. Similarly, at zero potential ($U = 0$ V vs NHE), the rds on N-substituted $\text{Co}_3\text{O}_4(311)$ is 0.74 eV uphill, smaller than on $\text{Co}_3\text{O}_4(311)$ (0.86 eV). By applying an overpotential of 0.46 V ($U = 0.862$ V vs NHE), all of the free energy steps for OER intermediates become negative and the free energy for the fourth step on $\text{Co}_3\text{O}_4(311)$ is more negative (-1.31 vs -0.68 eV) than that on N-substituted $\text{Co}_3\text{O}_4(311)$, implying stronger chemical adsorption of O_2 . It is well known that the ideal thermodynamic free energy change of the OER intermediates should be zero, wherein no energy would be required to drive the reaction [43]. Thus, our DFT results suggest that the OER activity of Co_3O_4 is substantially enhanced by the strongly coupling with N-C frameworks, in agreement with our electrochemical experiments (Fig. 3a-c).

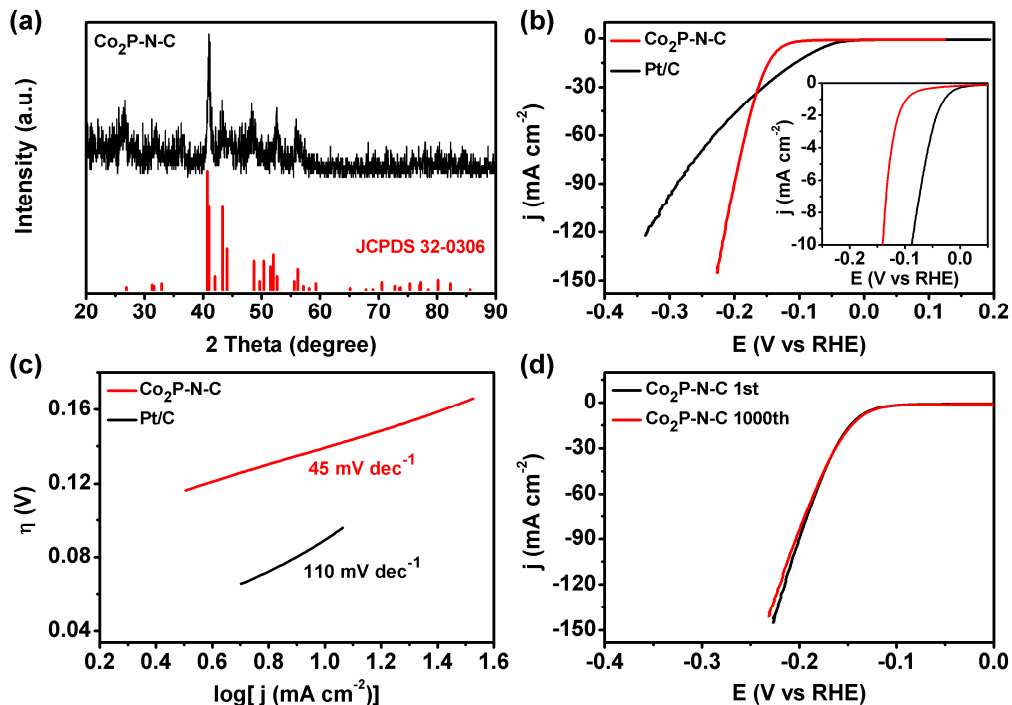


Fig. 5. (a) XRD pattern of $\text{Co}_2\text{P-N-C}$, (b) HER polarization curves of $\text{Co}_2\text{P-N-C}$ and commercial Pt/C in 1.0 M KOH at a scan rate of 5 mV s⁻¹ and 1600 rpm. (c) Tafel plots of $\text{Co}_2\text{P-N-C}$ and commercial Pt/C catalysts and (d) Stability tests of $\text{Co}_2\text{P-N-C}$ electrocatalyst through potential cycling, in which the polarization curves before and after 1000 potential cycles are displayed. The loadings of $\text{Co}_2\text{P-N-C}$ and commercial Pt/C are 0.4 mg cm⁻² and 51 $\mu\text{g cm}^{-2}$, respectively.

As revealed in Scheme 1b and Fig. S1, this molecular-confined gelation method is general to construct highly porous N-C frameworks with various strongly coupled metal oxides ($\text{MO}_x\text{-N-C}$). Furthermore, the resulting $\text{MO}_x\text{-N-C}$ frameworks can be used as precursors to prepare other derivatives for multiple electrocatalysis applications. For instance, the $\text{Co}_2\text{P-N-C}$ and $\text{Ni}_2\text{P-N-C}$ frameworks could be obtained for electrocatalytic HER via facile low-temperature phosphidation of

the corresponding $\text{MO}_x\text{-N-C}$ (see the Experimental section for details). Although multiple advanced nonprecious HER electrocatalysts were reported, most of them operated in strongly acidic media, wherein HER is thermodynamically more favorable [44-50]. However, OER is easier under basic conditions in view of the thermodynamics. As the overpotential loss for OER tends to be several-fold higher than that for HER, the efficiency of overall water splitting should be thermodynamically higher in basic electrolytes [45]. In addition, most earth-abundant OER catalysts are stable in alkaline electrolytes but vulnerable in acidic media [45-51]. In this regard, we were motivated to evaluate the HER activities of $\text{Co}_2\text{P-N-C}$ and $\text{Ni}_2\text{P-N-C}$ frameworks in alkaline electrolytes.

The XRD pattern and TEM images of $\text{Co}_2\text{P-N-C}$ confirm the formation of Co_2P (JCPDS No. 32-0306) in the hybrids (Fig. 5a and S4). The HER activity of $\text{Co}_2\text{P-N-C}$ was evaluated in 1.0 M KOH using a standard three-electrode system. Commercial Pt/C was also investigated side-by-side under the same condition. All the polarization curves (Fig. 5b) of two samples were obtained with a rotating disk electrode apparatus at a scan rate of 5 mV s⁻¹ and a rotation speed of 1600 rpm. $\text{Co}_2\text{P-N-C}$ at a loading amount of 0.4 mg cm⁻² exhibits excellent catalytic activity, showing sharp cathodic current density rise with increasing overpotentials. Specifically, $\text{Co}_2\text{P-N-C}$ requires an overpotential of 139 mV to reach a current density of 10 mA cm⁻², lower than those of reported nonprecious catalysts including $\text{MoC}_x\text{/C}$ (151 mV) [8], $\text{MoS}_{2+x}\text{/FTO}$ (310 mV) [52], NiFe LDH (>200 mV) [53], $\text{CoO}_x\text{@CN}$ (232 mV) [54], $\text{Ni}_2\text{P NPA/NF}$ (152 mV) [55], hp-Ni (181 mV) [56] and $\text{Ni}_2\text{P/Ti}$ (~200 mV) [57]. A more detailed comparison of various HER electrocatalytic parameters of $\text{Co}_2\text{P-N-C}$ and other reported catalysts is included in Table S2. The excellent HER activity of $\text{Co}_2\text{P-N-C}$ is also supported by its small Tafel slope of 45 mV dec⁻¹ (Fig. 5c), which is among the smallest Tafel slopes obtained for nonprecious HER catalysts in alkaline media (Table S2) and even lower than that of Pt/C catalysts (110 mV dec⁻¹) despite the latter show the negligible onset potential. Finally, the polarization curve for $\text{Co}_2\text{P-N-C}$ after 1000 continuous potential cycles overlay almost exactly with the initial one, implying its robust durability for long-term H_2 evolution (Fig. 5d). Similarly, the $\text{Ni}_2\text{P-N-C}$ frameworks could be also obtained for electrocatalytic HER via low-temperature phosphidation of the corresponding precursor. The TEM images (Fig. S5) and XRD pattern (Fig. S6a) cooperatively corroborate the successful realization of Ni_2P embedded in porous N-C frameworks. The electrocatalytic measurements for $\text{Ni}_2\text{P-N-C}$ under the same conditions reveal the high HER activity, small Tafel slope and robust stability (Fig. S6b-d).

3. Conclusions

In summary, we have developed a versatile, homogeneous, and especially facile molecular-confining route to construct strongly coupled metal oxides and N-C frameworks with interconnected configuration. By simply chelating various 1st-row transition metal ions with EDTA in agarose hydrogel followed by pyrolysis under inert atmosphere, we successfully synthesized diverse metal oxides-N-C networks featuring high specific surface area (metal oxides include Co_3O_4 , NiO_x , MnO_x ,

NiCo_xO_y and NiMn_xO_y) for electrocatalytic water splitting. As a representative example, $\text{Co}_3\text{O}_4\text{-N-C}$ shows great OER activity, rivaling the commercial RuO_2 catalysts. DFT calculations reveal that the strong coupling between N-C and Co_3O_4 is able to provide suitable binding sites for OER intermediates, beneficial to the overall O_2 evolution. Moreover, $\text{Co}_2\text{P-N-C}$ and $\text{Ni}_2\text{P-N-C}$ derived from the corresponding precursors also exhibit excellent HER performance, further highlighting the great versatility and broad application of our synthetic strategy.

4. Experimental Section

4.1 Materials synthesis

4.1.1 Synthesis of $\text{Co}_3\text{O}_4\text{-N-C}$ frameworks

The $\text{Co}_3\text{O}_4\text{-N-C}$ frameworks were prepared by a versatile, homogeneous and especially facile molecular-confining route. In a typical preparation, 1.69 g cobalt (II) acetate tetrahydrate containing 0.4 g Co^{2+} was added into 20 mL KOH aqueous solution buffer ($\text{pH} \sim 11$) containing 2.53 g EDTA to form the $\text{Co}^{2+}\text{-EDTA}$ complex before 0.4 g agarose was added (the molar ratio of metal ions and EDTA was kept at 1:1). Upon heating to boiling within 5 min, the agarose was dissolved to form a viscous and clear solution. This solution was allowed to cool down to room temperature so that a homogeneous hydrogel containing all the necessary chemical components was obtained. The agarose-based hydrogel was then freeze-dried, and the dehydrated monolith was subjected to a thermal treatment at 600 °C for 3 h in an argon flow. The as-prepared carbon materials were washed by deionized water and dried at 80 °C in vacuum to get $\text{Co}_3\text{O}_4\text{-N-C-600-1}$ (denoted as $\text{Co}_3\text{O}_4\text{-N-C}$ for brevity). “ $\text{Co}_3\text{O}_4\text{-N-C-x-y}$ ” denotes cobalt oxide-nitrogen-carbon frameworks, wherein the x represents the calcination temperature and y represents the mass ratio of the metal ion (Co^{2+}) and agarose. A series of cobalt oxide-nitrogen-carbon frameworks, such as $\text{Co}_3\text{O}_4\text{-N-C-450-1}$, $\text{Co}_3\text{O}_4\text{-N-C-700-1}$, $\text{Co}_3\text{O}_4\text{-N-C-600-0.5}$, $\text{Co}_3\text{O}_4\text{-N-C-600-2}$, can be obtained by changing the amount of agarose and the calcination temperature.

4.1.2 Synthesis of N-C frameworks-free counterpart (Co_3O_4)

To highlight the contribution of the in-situ incorporated N-C frameworks to the OER catalytic activity, the resulting $\text{Co}_3\text{O}_4\text{-N-C-600-1}$ was further subjected to calcination in air to eliminate nitrogen and carbon species, which also exhibited 3 D porous nanostructure (Fig. 1e and f).

4.1.3 Synthesis of Co_3O_4 -free N-C frameworks (N-C) and EDTA-free counterpart

To show the contribution of Co_3O_4 to OER catalytic activity and the molecular confinement of EDTA, the N-C frameworks without Co_3O_4 and EDTA-free counterpart were prepared. The procedures are similar to that of $\text{Co}_3\text{O}_4\text{-N-C-600-1}$ without involving cobalt (II) acetate tetrahydrate and EDTA, respectively.

4.1.4 Synthesis of $\text{Co}_3\text{O}_4\text{+N-C}$ sample

To exhibit the contribution of strongly interaction between Co_3O_4 and N-C frameworks in our Co_3O_4 -N-C catalyst, the Co_3O_4 +N-C sample was prepared. The agarose hydrogel was firstly prepared by adding 0.4 g agarose into 20 mL H_2O and subsequently gelation. After drying, the resulting samples were impregnated into 20 mL KOH aqueous solution buffer ($\text{pH} \sim 11$) containing the Co^{2+} -EDTA complex, the amounts of which is same as that of Co_3O_4 -N-C-600-1. Then, the resulting samples was dried again and calcined at 600 °C for 3 h in an argon flow.

4.1.5 Synthesis of other metal oxide-N-C and their-derived metal phosphide-N-C frameworks

Owing to the coordination versatility of EDTA with transition metal ions, this molecular-confined gelation method is very general to construct hydrogels with other metal oxides and/or their mixture (Scheme 1b) as well as the corresponding meteal oxides-nitrogen-carbon frameworks (e.g., MnO_x , NiO_x , NiCo_xO_y and NiMn_xO_y , Fig. S1) by simply changing the species of metal ions and the corresponding carbonization temperature for multiple electrocatalysis application. The resulting metal oxides-N-C samples could be further transferred to the corresponding metal phosphides-N-C frameworks for electrocatalytic HER. The Co_2P -N-C and Ni_2P -N-C can be obtained through a low-temperature phosphidation by using the resulting metal oxides-N-C frameworks as precursors. For example, Co_3O_4 -N-C and NaH_2PO_2 were put at two separate positions in a porcelain boat with NaH_2PO_2 at the upstream side of the furnace. The molar ratio for Co to P is 1:10. Subsequently, the samples were heated at 300 °C for 60 min in a static Ar atmosphere, and then naturally cooled to ambient temperature under Ar. The Ni_2P -N-C can be obtained through the similar low-temperature phosphidation.

4.2 Physical methods

Transmission electron microscopy (TEM) images were taken on a JEM 2100F microscope (JEOL, Japan) operated at 200 kV. Scanning electron microscopy (SEM) imaging was carried out on a Sirion 200 microscope (FEI, USA) operated at 5 kV. Nitrogen sorption isotherms were obtained at 77 K with a Micromertics ASAP 3020 analyzer (Micromertics, USA). Before each measurement, the sample was degassed in vacuum at 200 °C for at least 5 h. The Brunauer-Emmett-Teller (BET) method was used to calculate the specific surface area of the sample. The Barrett-Joyner-Halenda (BJH) model was utilized to analyze pore size distribution, based on which total pore volumes could be obtained. Powder X-ray diffraction (XRD) data were collected with a MiniFlex 600 diffractometer (Rigadu, Japan) using $\text{Cu K}\alpha$ radiation (40 kV, 15 mA). The X-ray photoelectron spectra (XPS) were recorded on an ESCALab MKII X-ray photo-electron spectrometer using $\text{Mg K}\alpha$ radiation as an exciting source.

4.3 Electrocatalytic measurements

The catalyst ink was prepared by ultrasonically mixing 4 mg of pre-grounded catalyst powder in 1 mL of 0.2 % Nafion (Sigma-Aldrich) aqueous solution for 30 min to form a homogeneous suspension of the catalyst particles. 20 μL of the catalyst ink was pipetted onto a polished glassy carbon rotational disk electrode (RDE), corresponding to a catalyst loading of $\sim 0.40 \text{ mg cm}^{-2}$. For comparison purpose,

commercially obtained Pt/C catalyst (20 wt%, Johnson Matthey) and RuO₂ catalysts were loaded with the same mass loading (~0.40 mg cm⁻²) for OER.

Electrochemical measurements with RDE were carried out with a conventional three-electrode cell system at room temperature. A computer-controlled electrochemical workstation (CHI760E, Chenhua Inc., China) was employed for all electrochemical tests. A glassy carbon RDE (PINE, 5 mm diameter) loaded with different electrocatalysts was used as the working electrode, an Ag/AgCl electrode as the reference electrode, and a Pt wire as the auxiliary electrode. All potentials reported in our work were quoted with respect to reversible hydrogen electrode (RHE) through RHE calibration described in the Supporting Information. The current density was normalized to the geometrical surface area and was iR corrected. The impedance measurements were performed in the same configuration at open circuit potential over a frequency range from 100 kHz to 1 mHz at the amplitude of the sinusoidal voltage of 5 mV and room temperature.

The OER activities of different catalysts were characterized in an O₂ saturated 0.1 M KOH electrolyte at room temperature. The flow of O₂ was maintained over the electrolyte (0.1 M KOH) during electrochemical measurements in order to ensure the O₂/H₂O equilibrium at 1.23 V vs. RHE.¹⁷ The potential was scanned from +0.4 to +0.9 V vs Ag/AgCl at a scan rate of 5 mV s⁻¹ and a rotation speed of 1600 rpm. Onset potential was determined based on the beginning of linear regime in the Tafel plot. The accelerated stability tests were performed in O₂-saturated 0.1 M KOH at room temperature by potential cycling at a sweep rate of 200 mV s⁻¹ for given number of cycles. At the end of each cycling, the resulting electrode was used for polarization and CV curves.

The HER activities of different catalysts were characterized in a H₂ saturated 1 M KOH electrolyte at room temperature. The high purity H₂ was constantly purged into the electrolyte to maintain a constant Nernst potential for H⁺/H₂ redox couple.⁵⁸ The potential was scanned from -0.9 to -1.4 V vs Ag/AgCl at a scan rate of 5 mV s⁻¹ and rotation speeds of 1600 rpm.

4.4 Theoretical computation methods

Spin-polarized DFT+U calculations were performed through the projector augmented wave (PAW) method as implemented in the Vienna ab initio simulation package (VASP). Please see the Supporting Information for more details.

Acknowledgements

Y.S. acknowledges the support of Utah State University and the National Science Foundation (CHE-1653978). D.J. is supported by the University of California, Riverside. This research used resources of the National Energy Research Scientific Computing Center, a DOE Office of Science User Facility supported by the Office of Science of the U.S. Department of Energy under Contract No. DE-AC02-05CH11231. B. Y thanks the support of Prof. Zhaoxiang Deng.

Appendix A. Supplementary material

Supplementary data associated with this article can be found in the online version at

References

- [1] S. Chu, A. Majumdar, *Nature* 488 (2012) 294-303.
- [2] B. You, Y. Sun, *Acc. Chem. Res.* 51 (2018) DOI: 10.1021/acs.accounts.8b00002.
- [3] Y. Jiao, Y. Zheng, M. Jaroniec, S. Z. Qiao, *Chem. Soc. Rev.* 44 (2015) 2060-2086.
- [4] X. Zheng, B. Zhang, D. D. Luna, Y. Liang, R. Comin, O. Voznyy, L. Han, F. P. G. Arquer, M. Liu, C. T. Dinh, T. Regier, J. J. Dynes, S. He, H. L. Xin, H. Peng, D. Prendergast, X. Du, E. H. Sargent, *Nat. Chem.* 10 (2018) 149-154.
- [5] B. You, Y. Sun, *ChemPlusChem* 81 (2016) 1045-1055.
- [6] I. Katsounaros, S. Cherevko, A. R. Zeradjanin, K. J. J. Mayrhofer, *Angew. Chem. Int. Ed.* 53 (2014) 102-121.
- [7] Y. Y. Liang, Y. G. Li, H. L. Wang, H. J. Dai, *J. Am. Chem. Soc.* 135 (2013) 2013-2036.
- [8] H. B. Wu, B. Y. Xia, L. Yu, X. Y. Yu, X. W. Lou, *Nat. Commun.* 6 (2015) 6512.
- [9] H. Hu, B. Y. Guan, B. Y. Xia, X. W. Lou, *J. Am. Chem. Soc.* 137 (2015) 5590-5595.
- [10] B. You, X. Liu, G. Hu, S. Gul, J. Yano, D-e, Jiang, Y. Sun, *J. Am. Chem. Soc.* 139 (2017) 12283-12290.
- [11] J. K. Nørskov, T. Bligaard, J. Rossmeisl, C. H. Christensen, *Nat. Chem.* 1 (2009) 37-46.
- [12] K. C. Leonard and A. J. Bard, *J. Am. Chem. Soc.* 135 (2013) 15885-15889.
- [13] J. Kibsgaard, T. F. Jaramillo, F. Besenbacher, *Nat. Chem.* 6 (2014) 248-253.
- [14] G. Jia, W. Zhang, G. Fan, Z. Li, D. Fu, W. Hao, C. Yuan, Z. Zou, *Angew. Chem. Int. Ed.* 56 (2017) 13781-13785.
- [15] Y. Zheng, Y. Jiao, Y. H. Zhu, L. H. Li, Y. Han, Y. Chen, A. J. Du, M. Jaroniec, S. Z. Qiao, *Nat. Commun.* 5 (2014) 3783.
- [16] L. Zhang, J. Xiao, H. Wang, M. Shao, *ACS Catal.* 7 (2017) 7855-7865.
- [17] T. Y. Ma, S. Dai, M. Jaroniec, S. Z. Qiao, *J. Am. Chem. Soc.* 136 (2014) 13925-13931.
- [18] E. J. Popczun, C. G. Read, C. W. Roske, N. S. Lewis, R. E. Schaak, *Angew. Chem. Int. Ed.* 53 (2014) 5427-5430.
- [19] Y. Gorlin, C. J. Chung, J. D. Benck, D. Nordlund, L. Seitz, T. C. Weng, D. Sokaras, B. M. Clemens, T. F. Jaramillo, *J. Am. Chem. Soc.* 136 (2014) 4920-4926.
- [20] J. Suntivich, K. J. May, H. A. Gasteiger, J. B. Goodenough, Y. Shao-Horn, *Science* 334 (2011) 1383-1385.
- [21] J. Hwang, R. R. Rao, L. Giordano, Y. Katayama, Y. Yu, Y. Shao-Horn, *Science* 358 (2017) 751-756.
- [22] Y. Y. Liang, Y. G. Li, H. L. Wang, J. G. Zhou, J. Wang, T. Regier, H. J. Dai, *Nat. Mater.* 10 (2011) 780-786.
- [23] M. Gong, W. Zhou, M. C. Tsai, J. G. Zhou, M. Y. Guan, M. C. Lin, B. Zhang, Y. F. Hu, D. Y. Wang, J. Yang, S. J. Penycook, B. J. Hwang, H. J. Dai, *Nat. Commun.* 5 (2014) 4695.
- [24] F. Meng, H. Zhong, D. Biao, J. Yan, X. Zhang, *J. Am. Chem. Soc.* 138 (2016) 10226-10231.

[25] P. Chen, T. Zhou, L. Xing, K. Xu, Y. Tong, H. Xie, L. Zhang, W. Yan, W. Chu, C. Wu, Y. Xie, *Angew. Chem. Int. Ed.* 56 (2017) 610-614.

[26] Y. Zheng, Y. Jiao, Y. Zhu, Q. Cai, A. V. Vasileff, L. H. Li, Y. Han, Y. Chen, S. Z. Qiao, *J. Am. Chem. Soc.* 139 (2017) 3336-3339.

[27] F. Zhao, Y. Shi, L. Pan, G. Yu, *Acc. Chem. Res.* 50 (2017) 1734-1743.

[28] B. You, P. Yin, J. Zhang, D. He, G. Chen, F. Kang, H. Wang, Z. Deng, Y. Li, *Sci. Rep.* 5 (2015) 11739.

[29] F. A. Westerhaus, R. V. Jagadeesh, G. Wienhöfer, M. M. Pohl, J. Radnik, A. E. Surkus, J. Rabeah, K. Junge, M. Nielsen, A. Brüchner, M. Beller, *Nat. Chem.* 5 (2013) 537-543.

[30] B. You, P. Yin, L. N. An, *Small* 10 (2014) 4352-4361.

[31] W. Li, J. P. Yang, Z. X. Wu, J. X. Wang, B. Li, S. S. Feng, Y. H. Deng, F. Zhang, D. Y. Zhao, *J. Am. Chem. Soc.* 134 (2012) 11864-11867.

[32] B. You, L. L. Wang, N. Li, C. L. Zheng, *ChemElectroChem* 1 (2014) 772-778.

[33] S. Bai, C. M. Wang, M. S. Deng, M. Gong, Y. Bai, J. Jiang, Y. J. Xiong, *Angew. Chem. Int. Ed.* 53 (2014) 12120-12124.

[34] J. Li, S. B. Tang, L. Lu, H. C. Zeng, *J. Am. Chem. Soc.* 129 (2007) 9401-9409.

[35] Y. Bai, W. H. Zhang, Z. H. Zhang, J. Zhou, X. J. Wang, C. M. Wang, W. X. Huang, J. Jiang, Y. J. Xiong, *J. Am. Chem. Soc.* 136 (2014) 14650-14653.

[36] H. Chen, W. G. Zhu, D. Xiao, Z. Y. Zhang, *Phys. Rev. Lett.* 107 (2011) 056804.

[37] X. X. Zou, A. Goswami, T. Asefa, *J. Am. Chem. Soc.* 135 (2013) 17242-17245.

[38] M. R. Gao, Y. F. Xu, J. Jiang, Y. R. Zheng, S. H. Yu, *J. Am. Chem. Soc.* 134 (2012) 2930-2933.

[39] T. Y. Ma, S. Dai, M. Jaroniec, S. Z. Qiao, *Angew. Chem. Int. Ed.* 53 (2014) 7281-7285.

[40] W. Niu, Z. Li, K. Marcus, L. Zhou, Y. Li, R. Ye, K. Liang, Y. Yang, *Adv. Energy Mater.* 8 (2018) 1701642.

[41] G. Li, X. Wang, J. Fu, J. Li, M. G. Park, Y. Zhang, G. Lui, Z. Chen, *Angew. Chem. Int. Ed.* 55 (2016) 4977-4982.

[42] B. Zhao, L. Zhang, D. Zhen, S. Yoo, Y. Ding, D. Chen, Y. Chen, Q. Zhang, B. Doyle, X. Xiong, M. Liu, *Nat. Commun.* 8 (2017) 14586.

[43] H. Fei, J. Dong, Y. Feng, C. S. Allen, C. Wan, B. Voloskiy, M. Li, Z. Zhao, Y. Wang, H. Sun, P. An, W. Chen, Z. Guo, C. Lee, D. Chen, I. Shakir, M. Liu, T. Hu, Y. Li, A. I. Kirkland, X. Duan, Y. Huang, *Nat. Catal.* 1 (2018) 63-72.

[44] T. Ling, D. Y. Yan, Y. Jiao, H. Wang, Y. Zheng, X. Zheng, J. Mao, X. W. Du, Z. Hu, M. Jaroniec, S. Z. Qiao, *Nat. Commun.* 7 (2016) 12876.

[45] N. Jiang, B. You, M. L. Sheng, Y. Sun, *Angew. Chem. Int. Ed.* 54 (2015) 6251-6254.

[46] N. Jiang, B. You, M. Sheng, Y. Sun, *ChemCatChem* 8 (2016) 106-112.

[47] B. You, Y. Sun, *Adv. Energy Mater.* 6 (2016) 1502333.

[48] B. You, N. Jiang, M. Sheng, M. W. Bhushan, Y. Sun, *ACS Catal.* 6 (2016) 714-721.

[49] B. You, N. Jiang, M. Sheng, S. Gul, J. Yano, Y. Sun, *Chem. Mater.* 27 (2015) 7636-7642.

[50] Y. Yang, H. Fei, G. Ruan, J. M. Tour, *Adv. Mater.* 27 (2015) 3175-3180.

[51] B. You, X. Liu, N. Jiang, Y. Sun, *J. Am. Chem. Soc.* 138 (2016) 13639-13646.

[52] C. G. Morales-Guio, L. Liardet, M. T. Mayer, S. D. Tilley, M. Grätzel, X. L. Hu, *Angew. Chem. Int. Ed.* 54 (2015) 664-667.

[53] J. S. Luo, J. H. Lim, M. T. Mayer, M. Schreier, M. K. Nazeeruddin, N. G. Park, S. D. Tilley, H. J. Fan, M. Grätzel, *Science* 345 (2014) 1593-1596.

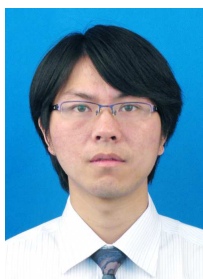
[54] H. Y. Jin, J. Wang, D. F. Su, Z. Z. Wei, Z. F. Pang, Y. Wang, *J. Am. Chem. Soc.* 137 (2015) 2688-2694.

[55] B. You, N. Jiang, X. Liu, Y. Sun, *Angew. Chem. Int. Ed.* 55 (2016) 9913-9917.

[56] B. You, X. Liu, X. Liu, Y. Sun, *ACS Catal.* 7 (2017) 4564-4570.

[57] E. J. Popczun, J. R. McKone, C. G. Read, A. J. Biacchi, A. M. Wiltrot, N. S. Lewis, R. E. Schaak, *J. Am. Chem. Soc.* 135 (2013) 9267-9270.

[58] T. Tang, W. J. Jiang, S. Niu, N. Liu, H. Luo, Y. Y. Chen, S. F. Jin, F. Gao, L. J. Wan, J. S. Hu, *J. Am. Chem. Soc.* 139 (2017) 8320-8328.



Dr. Bo You received his B.S. degree in Chemistry from Heilongjiang University in 2008 and a Ph.D. degree under the supervision of Prof. Zhaoxiang Deng at University of Science and Technology of China (USTC) in 2014. Subsequently, he conducted the postdoctoral research in Prof. Yujie Sun's group at Utah State University, Prof. Hong Li's group at Nanyang Technological University and now in Prof. Shi-Zhang Qiao's group at The University of Adelaide. His research focuses on interface catalysis for advanced renewable energy (ICARE).



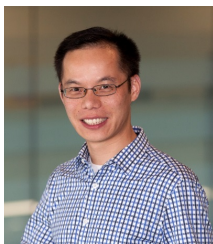
Yadong Zhang is a Ph.D. student under the supervision of Professor Ruifeng Lu at Nanjing University of Science and Technology (NUST), and a visiting student under the supervision of Professor De-en Jiang at University of California, Riverside (UCR). His research interests are theoretical research on electrochemistry, supercapacitor and gas separation.



Peiqun Yin received her Ph.D. degree under the supervision of Professor Yuen Wu at University of Science and Technology of China (USTC) and Yadong Li at Tsinghua University, and now is a Postdoc under the supervision of Professor Hua Zhang at Nanyang Technological University, Singapore. Her research interests are non-precious nanomaterials on energy conversion and storage.



De-en Jiang is a tenured associate professor in Department of Chemistry, University of California, Riverside. He received his B.S. and M.S. degrees from Peking University and his Ph.D. degree from University of California, Los Angeles (UCLA), all in chemistry. He joined Oak Ridge National Laboratory first as a postdoctoral research associate and then became a research staff member. He moved to University of California, Riverside in July 2014. His research focuses on applying state-of-the-art computational methods to important chemical systems and energy-relevant problems.



Yujie Sun received a B.S. degree in Chemistry from Fudan University in 2005. He then pursued graduate studies in inorganic photochemistry with Prof. Claudia Turro at The Ohio State University and received a Ph.D. degree in 2010. Subsequently, he joined the group of Prof. Chris Chang at the University of California, Berkeley and Lawrence Berkeley National Laboratory for postdoctoral studies. In 2013, Yujie started his independent career as an assistant professor at Utah State University. He received the Ralph E. Powe Junior Faculty Enhancement Award in 2015 and the NSF CAREER Award in 2017. His group is interested in developing and understanding inexpensive materials and complexes for energy catalysis and biomedical applications.

Graphical Abstract

A universal, homogeneous, and especially facile molecular-confining route was reported to synthesize strongly coupled transition metal oxides-N-C frameworks with interconnected configuration as advanced nonprecious electrocatalysts for water splitting.

